CRITICAL NUMBER OF SPACECRAFT IN LOW EARTH ORBIT: A NEW ASSESSMENT OF THE STABILITY OF THE ORBITAL DEBRIS ENVIRONMENT

Hugh G. Lewis[(1)] and Donald J. Kessler[(2)]

[(1)] University of Southampton, Faculty of Engineering and Physical Sciences, Boldrewood Innovation Campus, Southampton SO16 7QF, United Kingdom, Email: hglewis@soton.ac.uk
[(2)] Consultant, Asheville, North Carolina, United States of America

ABSTRACT

The stability model by Kessler and Anz-Meador identified regions near 900 km and 1400 km where the number of intact objects in the February 1999 satellite catalogue exceeded the critical number needed for a runaway environment. The deployment of large constellations of satellites in low Earth orbit, has prompted a new analysis with this approach. Using data from on-orbit fragmentation events, this paper introduces a revised stability model for altitudes below 1020 km and evaluates the March 2025 population of payloads and rocket stages to identify new regions of instability. The results indicate the current population of intact objects exceeds the unstable threshold at all altitudes between 400 km and 1000 km and the runaway threshold at nearly all altitudes between 520 km and 1000 km. Planned deployments of large constellations will likely lead to the population of intact objects across an even greater extent of low Earth orbit exceeding the runaway threshold.

1 INTRODUCTION

In 2001, Kessler and Anz-Meador presented a stability model for evaluating the critical number of spacecraft in low Earth orbit (LEO) and identified regions of instability where the number of intact objects exceeded the threshold for an unstable environment and a possible region of instability where the number exceeded the threshold for a runaway environment [1]. Fig. 1 shows the number of intact objects found between the given altitude and an altitude of 1020 km in the February 1999 catalogue and the threshold numbers for a runaway environment and for an unstable environment from the stability model in [1]. Kessler and Anz-Meador concluded that where the number of intact objects exceeded these thresholds, maintaining this population of intact objects would cause the fragment population to increase. If the number of intact objects exceeds the unstable threshold, the increase will be either to a higher but eventually stable value or, if the number of intact objects exceeds the runaway threshold, the fragment population will run away over an infinite amount of time to an infinite number of fragments. Kessler and Anz-Meador found the region between 600 km and 1000 km to be well above the unstable threshold and the region between 800 km and 970 km to be above the runaway threshold.

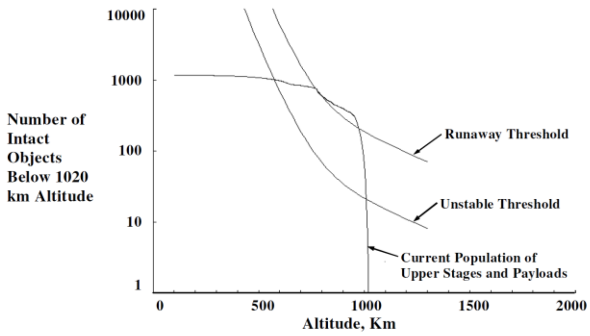

Figure 1. Possible Regions of Instability Below 1020 km (February 1999 Catalogue) from [1].

The results in [1] also showed that the region between 1300 km and 1420 km was above the runaway threshold and the entire region between 1000 km and 1500 km was above the unstable threshold (Fig. 2).

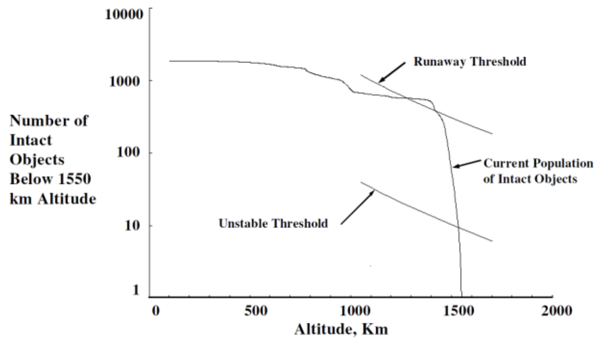

Figure 2. Regions of Instability Below 1550 km (February 1999 Catalogue) from [1].

Since the publication of these results, simulation studies undertaken using semi-deterministic, Monte Carlo, evolutionary models have predicted runaway fragment population growth in the same altitude regions identified by Kessler and Anz-Meador [2-3]. Furthermore, the population of spacecraft in LEO has seen significant growth in the two decades since their work. At the time the results from [1] were presented, the number of active

Proc. 9th European Conference on Space Debris, Bonn, Germany, 1–4 April 2025, published by the ESA Space Debris Office
Editors: S. Lemmens, T. Flohrer & F. Schmitz, (http://conference.sdo.esoc.esa.int, April 2025)

spacecraft in Earth orbits was about 1000. The current number of active spacecraft is nearly 12,000 (Fig. 3). The unprecedented growth in the number of spacecraft has been driven primarily by the deployment of satellites into large constellations in LEO.

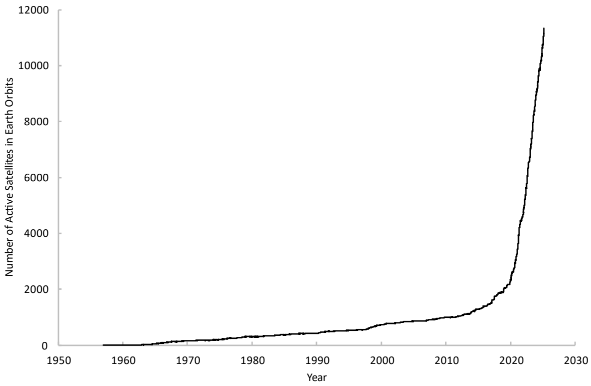

Figure 3. History of Active Satellites from Jonathan's Space Pages[1].

Fig. 4 gives the spatial density of intact objects from the February 1999 catalogue, consistent with the timeframe used in [1], and for those in orbit on 28 March 2025. Kessler and Anz-Meador identified four regions of interest with high concentrations of intact objects: (1) 570 km to 670 km, (2) 750 km to 860 km, (3) 920 km to 1020 km, and (4) 1350 km to 1550 km. In the February 1999 catalogue the Iridium constellation at 780 km was the cause of a peak in region 2. Whilst these regions are still visible in the spatial density plot for intact objects in orbit on 28 March 2025, the Starlink constellation is the cause of peaks between about 350 km and 550 km and the OneWeb constellation is the cause of a peak at 1200 km.

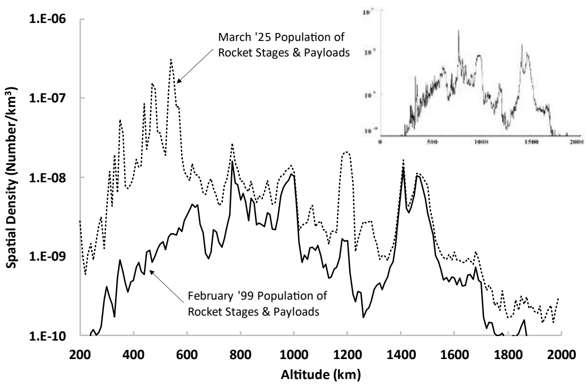

Figure 4. Spatial Density of Intact Objects, February 1999 and March 2025. Inset Figure Shows the Result for February 1999 from [1].

Fig. 5 gives the spatial density of payloads and upper stages independently for February 1999 and Fig. 6 gives the same for March 2025. The first shows the spatial density of each being about equal in February 1999 with the same concentrations as the solid line in Fig. 4. The second shows that very little change in the distribution of spatial density of upper stages has occurred since 1999. In contrast, the second figure shows the clear dominance of payloads in the current spatial density profile. It also shows an increase in utilisation of space below 1200 km.

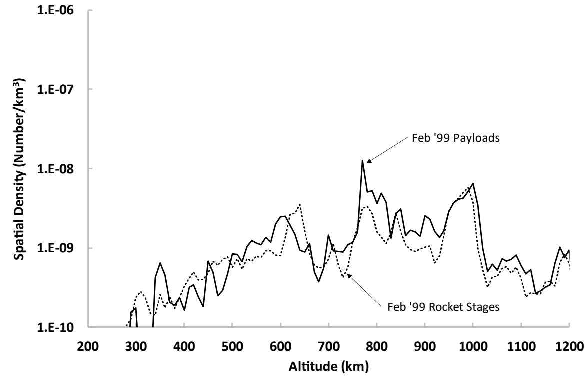

Figure 5. Spatial Density of Payloads and Rocket Stages Below 1200 km, February 1999.

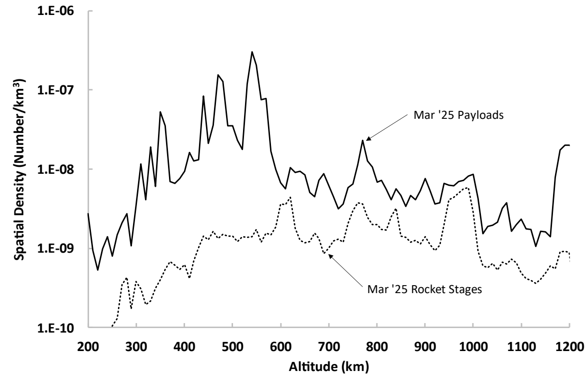

Figure 6. Spatial Density of Payloads and Rocket Stages, March 2025.

Based on the spatial density distribution for February 1999, Kessler and Anz-Meador previously suggested that the region below 670 km might be sufficiently low in altitude that atmospheric drag would remove fragments quickly and the spatial density concentration might not be important [1]. The change in the situation for this region, following the beginning of the deployment of the Starlink constellation, has prompted a new analysis of this region and those below about 1000 km.

New data from orbital collisions and a ground-based test will be used in this paper to update the stability model developed by Kessler and Anz-Meador and to evaluate the current population of intact objects against the "critical number" needed for an unstable environment

---

[1] Available at: https://planet4589.org/space/index.html

and for a runaway environment.

2 FRAGMENT DATA

The timing of the work reported in [1] meant that only fragment data from a USAF test could be used to resolve the key uncertainties in determining critical density. That test was conducted 13 September 1985 at an altitude of 525 km and involved the 850 kg satellite known as P-78 or Solwind. The satellite was struck with an approximately 16 kg projectile at 7 km/sec producing a total of 285 catalogued fragments, all of which re-entered within about 15 years. Analysis of the orbital elements in this data set enabled the calculation of the spatial density of collision fragments as a function of altitude at different times, without the need for assumptions involving area-to-mass or fragment velocities or an accurate atmospheric drag model. The premise of the work in [1] was that the results arising from the analysis of the P-78 fragments could be applied to breakups at different altitudes, adjusted for different solar activity conditions, and generalised to all collision fragments.

Since the P-78 test, other orbital tests and collisions have occurred, producing fragment data that can be used to improve the calculation of critical density.

In January 2007, the non-operational 750 kg Fengyun-1C spacecraft was hit at an altitude of 860 km by an estimated 600 kg kinetic kill vehicle at about 9 km/sec, creating more than 3,000 catalogued fragments [4]. In February 2009, the active 700-kg Iridium-33 spacecraft and the non-operational 900 kg Cosmos-2251 spacecraft collided at 780 km over Siberia with a relative speed of about 11.5 km/sec [5]. This collision represented the first orbital collision involving two intact objects and produced more than 2,000 catalogued fragments. Two further orbital tests have been conducted: the 740 kg Microsat-R satellite on 27 March 2019 at an altitude of 274 km and the 1,750 kg Cosmos-1408 satellite on 15 November 2021 at an altitude of about 485 km.

Radar cross-section (RCS) data from the Space Surveillance Network (SSN) are available for most of the catalogued P-78, Fengyun-1C, Iridium-33, and Cosmos-2251 fragments[2]. However, there are no RCS measurements for the Microsat-R or Cosmos-1408 readily available. The diameters of the fragments with RCS measurements can be estimated using NASA's Size Estimation Model (SEM; Fig. 7) [6]. Assuming diameter to be equivalent to the characteristic length, the fragment area can be calculated using the NASA Standard Breakup Model [7].

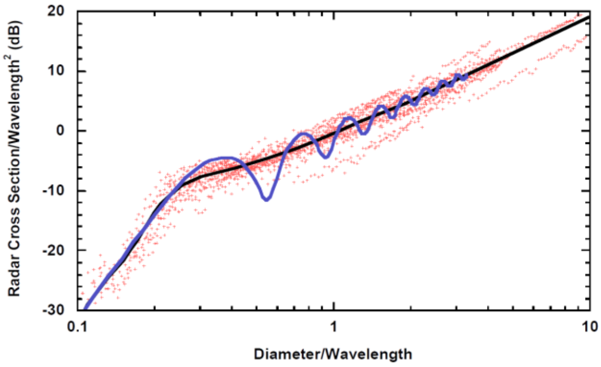

Figure 7. Results of RCS-to-Physical Size Measurements. Each Point Represents an Average RCS for a Single Object Measured at a Single Frequency Over Many Orientations. The Oscillating Line is the RCS for a Spherical Conductor While the Smooth Line is the Polynomial Fit to the Data [6].

Care must be taken in working with RCS values as they may reflect averaging, filtering, inappropriate application of the NASA SEM, or other systemic processing issues whose net effect is to render a relationship between the SEM characteristic length [6], the corresponding fragment area [7], and an estimated mass problematic. Specifically, fragments in the decimetre size range may be underestimated in size by a factor of up to 2, as can be seen in Fig. 8 when comparing the "SSN" curve against a model derived using RCS values prior to 2001 [8]. If the SEM size is underestimated, then the corresponding estimate of fragment mass will be similarly underestimated.

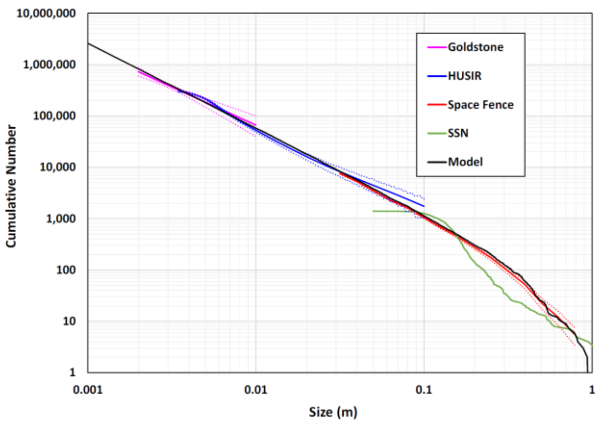

Figure 8. Cumulative Size Distribution of Cosmos-1408 Fragments Based on Different Measurement Data [8]. The Black Curve is the NASA Standard Breakup Model Prediction.

Fig. 9 shows a plot comparing the cumulative size distribution of the P-78 fragments derived from the SSN RCS data and the corresponding cumulative size

[2] Available at: https://keeptrack.space/

distribution of the Cosmos-1408 fragments derived from SSN (with data taken from Fig. 8). The P-78 test was conducted in 1985 and all fragments were catalogued and re-entered before the NASA SEM development timeframe. In contrast, fragments from the Cosmos-1408 breakup were catalogued two decades after the development of the SEM. As both breakups were collisions, the slopes should be approximately -1.71 as per the NASA Standard Breakup Model [7]. However, Fig. 9 shows anomalously smaller sizes for the Cosmos-1408 fragments in the decimetre region, resulting from the use of SSN-derived RCS measurements with the NASA SEM.

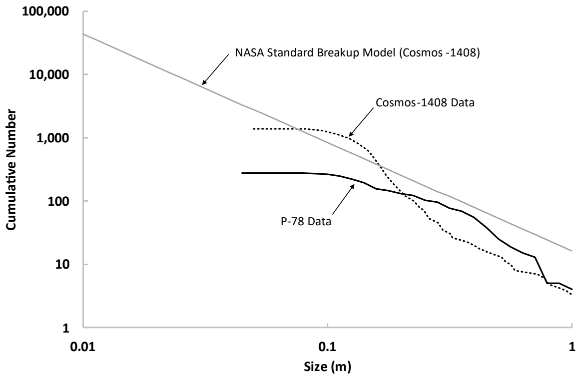

Figure 9. Comparison of the Cumulative Size Distributions of P-78 and Cosmos-1408 Fragments Based on SSN RCS Measurement Data and the NASA SEM. The Cosmos-1408 line is from Fig. 8 [8].

To account for the underestimation in the decimetre range, an approach for correcting the RCS-derived sizes was developed and subsequently applied to the Fengyun-1C, Iridium-33, and Cosmos-2251 fragments. SSN-derived RCS data were not available for the Cosmos-1408 fragments so, instead, the SSN-derived distribution in Fig. 6 was sampled to produce a data set of Cosmos-1408 fragment sizes. Through a simple, empirical optimisation approach that aimed to match the cumulative size distribution of the sampled fragments with the "Space Fence" and "Model" distribution in Fig. 8, a size correction was determined for fragments with sizes between 0.14 m and 1 m. The new size, D_{new}, for these fragments was estimated to be

$$D_{new} = D(1 + 0.8\sin(\pi\,|D - 0.57|/0.43)) \quad (1)$$

where D is the original fragment size derived from its SSN-RCS measurement using the NASA SEM. The first constant is a scale factor, the second is the midpoint of the identified size range, in metres, and the third constant is half the range, again in metres. Fig. 10 shows the effect of the correction in Eq. 1 on the cumulative size distribution of Cosmos-1408 fragments, with the distributions from Fig. 8 also shown for comparison.

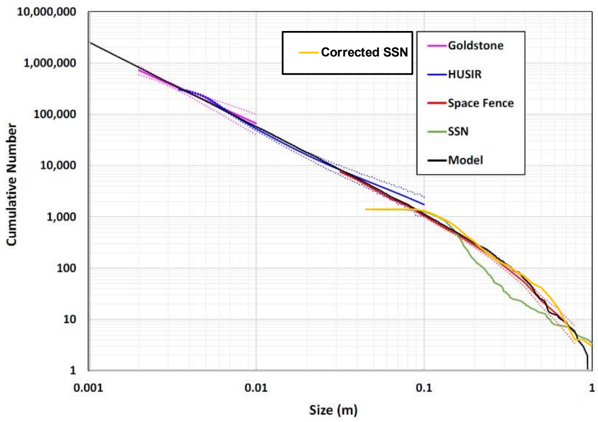

Figure 10. Cumulative Size Distribution of Cosmos-1408 Fragments for Different Measurement Data [8] Including a Correction for decimetre sizes derived from SSN-RCS Measurements and the NASA SEM.

Whilst [1] determined the fragment area-to-mass from the orbital decay history of the P-78 fragments, this was only made possible by the relatively small number of fragments produced by the P-78 test and the relatively short orbital lifetimes. The P-78 test was conducted at an altitude high enough that most of the fragments that were large enough to be catalogued, were catalogued, yet low enough that the fragments decayed out of orbit relatively quickly, offering a detailed and comprehensive time history. Given the higher altitudes of the Fengyun-1C and Iridium-33-Cosmos-2251 events, a significant proportion of the fragments produced have orbital lifetimes measured in decades or centuries. Furthermore, the large number of fragments (more than 5,000) and the large number of orbital element sets for each fragment would require a computationally- and time-intensive analysis effort. Hence, an alternative to the use of the orbital time history was considered. For consistency, this alternative was also applied to the P-78 fragment data.

The European Space Agency's Database and Information System Characterising Objects in Space (DISCOS) provides initial orbit information, decay dates, and re-entry predictions for the P-78, Fengyun-1C, Iridium-33, and Cosmos-2251 fragments[3]. This dataset provided the opportunity to estimate the fragment area-to-mass using an orbital propagator, which was part of the Debris Analysis and Monitoring Architecture to the Geosynchronous Environment (DAMAGE), developed at the University of Southampton. This process was conducted as follows:

[3] Available at: https://discosweb.esoc.esa.int/

1. For each fragment, the cross-section derived from its RCS, the initial mean altitude and predicted orbital lifetime from DISCOS, and an estimate of the atmospheric density from an exponential atmospheric model, were used to provide an initial estimate of the fragment area-to-mass ratio.
2. The initial estimate of the area-to-mass was bracketed by a value 100 times larger and a value 100 times smaller. The fragment was propagated using DAMAGE (assuming only atmospheric drag and J2 perturbations) for each of the lower, middle, and upper values of the area-to-mass and the remaining orbital lifetime was predicted for each case.
3. The difference between the predicted orbital lifetime and the lifetime obtained from DISCOS was used to identify the half of the bracket containing the "actual" area-to-mass ratio. A new middle value for the area-to-mass was calculated and used in a new propagation.
4. The process was repeated until the difference between the predicted and "actual" lifetime was below a tolerance (which varied for each fragment depending on its "actual" lifetime). The last middle value to be computed was used as the area-to-mass of the fragment.

With the area information from RCS data and area-to-mass from the fitting process described above, and under the assumptions and limitations associated with each, the mass of fragments from the breakup events were calculated. The size of the resulting fragment sample is detailed in Tab. 1.

Table 1. Number of Fragments with Mass Estimates Derived Through the Area-to-Mass Fitting Process as a Proportion of All Fragments Catalogued.

Spacecraft Name	**Number of Fragments with mass estimate**	**Number of catalogued fragments (DISCOS)**	**Proportion**
P-78	280	288	97%
Fengyun-1C	3,408	3,536	96%
Iridium-33	621	2,375	95%
Cosmos-2251	1,647		
Total	5,956	6,199	96%

The sum of the P-78 fragment masses was found to be 1,169 kg, which is larger than the mass of the spacecraft. As noted by [1], this error could result from the uncertainty in the calculation of the mass of relatively few large fragments or from atmospheric density or RCS bias. Discrepancies were also found with the fragment masses calculated for the other collisions, even following the application of the correction in Eq. 1. Therefore, all the masses were scaled, as detailed in Tab. 2.

Table 2. Scaling Factors Used to Align the Total Fragment Mass with the Satellite Mass. Satellites marked with an asterisk had a correction applied to fragments in the decimetre range to account for RCS-to-size underestimation.

Spacecraft Name	**Assumed Spacecraft Mass (kg)**	**Total Estimated Fragment Mass (kg)**	**Fragment Mass Scaling Factor**
P-78	850	1,169	1/1.4
*Fengyun-1C**	750	919	1/1.2
*Iridium-33**	700	379	1.8
*Cosmos-2251**	900	510	1.8

To provide some validation of the process used to derive the fragment mass data, Fig. 11 shows a plot of the log of the cumulative number of P-78 fragments as a function of log mass. The inset figure shows the corresponding plot from [1]. Both plots are approximately linear for fragments larger than about 1 kg and follow a collision breakup model where number varies as the ratio of fragment mass to target mass to a power of -0.8. For fragments smaller than 1 kg, the number increases at a lower rate in alignment with expectations around the sensitivity of the radar system.

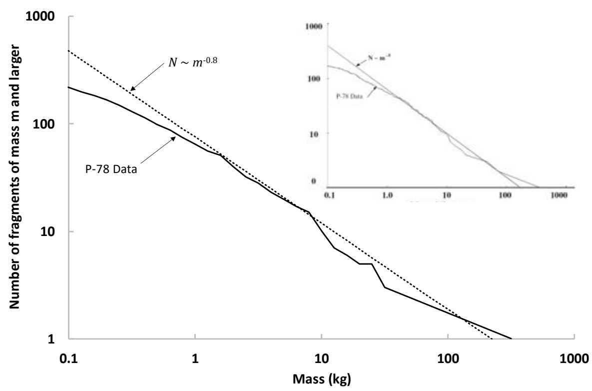

Figure 11. Cumulative Number of P-78 Catalogued Fragments as a Function of Mass. Inset Figure Shows the Result for January 1986 from [1].

Since the work reported in [1], a consortium from the US conducted a hypervelocity impact test at Air Force Arnold Engineering Development Complex (AEDC) of a 56-kg-class spacecraft known as "DebriSat", representative of modern LEO spacecraft [9]. The impact of the 570 g projectile at 6.8 km/sec produced more than 200,000 fragments over 2 mm in size. Whilst the fragment data set is not publicly available, the consortium has reported the cumulative number of fragments by characteristic length and mass. Additionally, another ground hypervelocity impact test reported in [1] was the Transit/OSCAR spacecraft during the SOCIT series of tests. This test impacted a 150 g projectile into the 35 kg Transit spacecraft.

For a collision to be catastrophic at 10 km/sec, the ratio of target mass to projectile mass should be less than 1250 [10]. Hence, a fragment mass greater than 0.68 kg would break up a spacecraft with the same mass as P-78. For Fengyun-1C, Iridium-33, Cosmos-2251, DebriSat, and Transit, the fragment masses needed would be 0.6 kg, 0.56 kg, 0.72 kg, 0.045 kg, and 0.028 kg, respectively.

Fig. 12 shows a plot of the log of the cumulative number of fragments as a function of log mass for the four orbital collisions and the ground hypervelocity impact test on DebriSat. The number of fragments varies as the ratio of fragment mass to target mass to a power somewhere between -0.6 and -0.9. Tab. 3 details the fragment masses capable of causing a catastrophic collision and the number of fragments found exceeding these levels. Across the six collisions considered, the average number of fragments with the necessary mass was found to be 101. However, the result is likely to be biased by Iridium-33, which is considerably "out of family" compared with the satellites of similar size, suggesting the possibility that not all the satellite mass was involved in its collision with Cosmos-2251. The median number of fragments with the necessary mass to catastrophically breakup a satellite with the same mass is 112, which is more representative. In contrast, [1] assumed the catastrophic collision of a satellite would produce about 90 fragments that are massive enough to catastrophically breakup another satellite of the same mass.

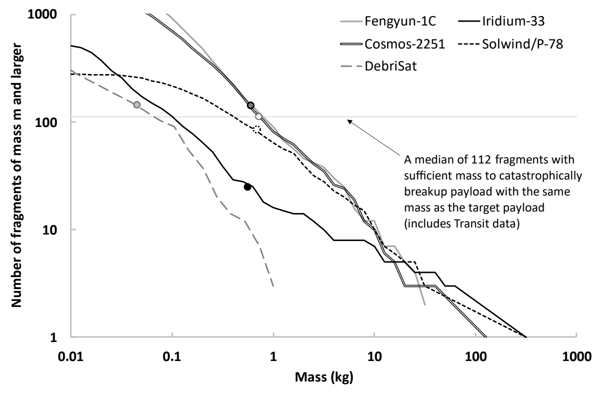

Figure 12. Cumulative Number of Catalogued Fragments as a Function of Mass for Five collision events. The Circles Show the Mass and Number of Fragments Capable of Causing a Catastrophic Collision for Each Satellite.

Table 3. Number of Fragments Needed to Breakup Another Payload with the Same Mass. An Average Value for Transit Is Included, Based on Data in [1].

Spacecraft Name	**Assumed Spacecraft Mass (kg)**	**Fragment Mass Needed for Breakup (kg)**	**Number of Fragments**
P-78	850	0.68	86
Fengyun-1C	750	0.6	142
Iridium-33	700	0.56	25
Cosmos-2251	900	0.72	112
DebriSat	56	0.045	145
Transit	35	0.028	95
Average	549	0.439	101
Median	750	0.6	112

Fig. 13 is a plot of the spatial density of the P-78, Fengyun-1C, Iridium-33, and Cosmos-2251 fragments six months after each collision. Each fragment was propagated using DAMAGE from the epoch of its addition into the catalogue to the six-month census date. This plot shows that the spatial density remains highest close to the breakup altitude. Fragments with masses that exceed the catastrophic collision threshold will be found much closer to the breakup altitude than the other less massive, catalogued fragments. Through calculation of the integral of spatial density over time, [1] showed that altitudes most affected are near the breakup altitude and the effect on lower altitudes is inversely proportional to the atmospheric density. Hence, collisions at higher altitudes are more important to a given altitude than collisions at lower altitudes. Fig. 13 supports the finding in [1] that the effects of collisions on all altitudes can be approximated by assuming that all the breakup fragments are in circular orbits.

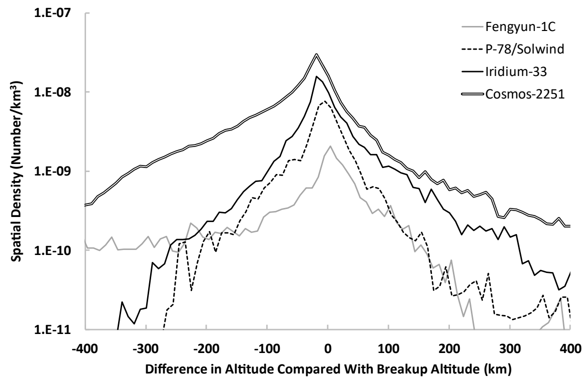

Figure 13. Estimation of the Spatial Density of Catalogued Fragments 6 Months After Each Collision.

Although several collisions and orbital tests have involved payloads, there is still little fragmentation data available on the hypervelocity breakup of upper stages. In April 2014, the ground-based DebrisLV hypervelocity impact test was conducted at AEDC Range G, as a companion test to DebriSat and to represent the full-scale hypervelocity impact behaviour of the current population of derelict launch vehicle upper stages in orbit. Whilst the impact of the 598 g projectile with 17 kg DebrisLV at 6.9 km/sec will have produced many fragments capable of catastrophically breaking up an upper stage of the same mass, no fragment data are currently available. Reference [1] analysed 3,605 explosion fragments from 15 explosions of upper stages in orbit to derive size, area, and mass characteristics. These were used in the development of the original stability model under the assumption that explosions can duplicate hypervelocity collisions. Reference [1] concluded that the number of upper stage fragments capable of causing a catastrophic collision was less than the equivalent number of payload fragments, determined from the P-78 collision.

From [1] and the analysis of collision data for P-78, Fengyun-1C, Iridium-33, Cosmos-2251, supplemented with results for DebriSat and Transit, the following conclusions are reached:

1. A catastrophic collision of a payload will produce about 112 fragments that are massive enough to catastrophically break up another payload of the same mass.
2. The orbits of these fragments are sufficiently close to the orbit of the original payload for a model to assume near-circular orbits for collision fragments.
3. The largest uncertainty in using a model to determine the stability of LEO is the continuing lack of hypervelocity collision data for upper stages.
4. A secondary source of uncertainty for the new stability model lies in the conversion of SSN RCS measurements to fragment sizes using the NASA SEM.

3 STABILITY MODEL

The stability model developed by [1] defined the environment at a point in space by assessing only the rate that objects pass through that point, assuming it to be the rate of orbital decay due only to atmospheric drag. This approach enabled a simple analytical expression for the critical number of objects to be evaluated at different altitudes, tying it to relevant and meaningful physical properties of the objects and environment and making it computationally efficient. This contrasts with most environment models, including those based on Monte Carlo simulation and system dynamics (so-called "source-sink" models), which employ many volume elements to evaluate stability and obtain accurate results.

The work presented in this paper uses the same stability model approach as [1], but with updated parameters based on analyses of the fragment and object data presented above. To support the reader, the reporting of the assumptions and development of the stability model in [1] are reproduced here, with some elaborations and minor corrections.

3.1 Model assumptions

Reference [1] assumed that above some altitude, h_1, the rate of breakups of intact spacecraft, dB/dt, is constant and producing fragments that decay through altitude h_1. Each collision was assumed to produce a time-dependent spatial density of $S_1(t)$ at h_1. The average spatial density of fragments, S_B, is then

$$S_B = \frac{dB}{dt} \int S_1(t)\, dt \tag{2}$$

where Eq. 2 is integrated over the time it takes for the fragments to pass through h_1. As noted in [1], the value of this integral could be obtained numerically from Fig. 2 in [1]. However, as shown below, a simpler analytical technique can be used due to the near-circular orbits assumed for the fragments.

The spatial density of intact spacecraft, S_i, and the spatial density of fragments large enough to catastrophically break up intact spacecraft, S_f, were assumed to be constant within a volume of ΔU above altitude h_1, and

$$\frac{dB}{dt} = S_i^2 \sigma_i V\, \Delta U + S_i S_f \sigma_f V\, \Delta U \tag{3}$$

where it was assumed that when two intact objects collide, two breakups occur. The collision cross-section, σ_i, of two intact objects of physical cross-section, A_i, is

$$\sigma_i = \left(A_i^{1/2} + A_i^{1/2}\right)^2 = 4A_i \tag{4}$$

and the collision cross-section, σ_f, between an intact object and a fragment with physical cross-section, A_f, is

$$\sigma_f = \left(A_i^{1/2} + A_f^{1/2}\right)^2 \tag{5}$$

V is the average relative velocity that transforms spatial density into flux and has a value of about 7.5 km/sec.

Finally, it was assumed that the environment is in equilibrium and the altitude of the volume above h_1 is similar to h_1, leading to the approximation $S_B = S_f$. In general, S_f will always be greater than S_B when the environment is in equilibrium and the number of intact objects is constant with altitude. Whilst this could be addressed by creating additional volume elements, this would add complexity and reduce transparency and flexibility. Hence the conservative assumption in [1] was that $S_B = S_f$.

3.2 Model development

The integral of spatial density over time, expressed in terms of the rate of change of the orbital semi-major axis, da/dt, for an elliptical orbit is the same as for circular orbits multiplied by a weighting factor, W. Therefore, the integral in Eq. 2, assuming N_0 fragments are produced by a single breakup is

$$\int S_1(t)\,dt = \sum \frac{W}{4\pi a^2 (da/dt)} \tag{6}$$

where the summation is for N_0 fragments massive enough to break up an intact spacecraft. The value of W is 1 for circular orbits and can be as high as 50 for some highly elliptical orbits. For the slightly elliptical orbits contained in the P-78 data in [1] and also seen in the Fengyun 1C, Iridium 33, and Cosmos 2251 data above, interpolation of data in [11] suggests that W would be most likely near 1.3 to 1.5 just after the collision and would approach 1 as the orbits decayed and circularised at lower altitudes.

The rate of change of the semi-major axis for circular orbits is derived from the drag force equation, an equation for the total energy of an orbit, and the equation in which energy loss is expressed as force applied through a distance (the 'work-energy' principle). The drag force, F_D, is

$$F_D = \frac{1}{2}\rho_a C_D V_o^2 \frac{A}{m} \tag{7}$$

where ρ_a is the atmospheric density, C_D is the drag coefficient (approximately 2.2), V_o is the orbital velocity, and A/m is the area-to-mass ratio. The total energy of an orbit is proportional to $1/a$. The resulting equation is

$$\frac{da}{dt} = a\rho_a C_D V_o \frac{A}{m} \tag{8}$$

Combining Eqs. 6 and 8,

$$\int S_1(t)\,dt = \frac{N_0 W (m/A)_a}{4\pi a^3 V_o \rho_a C_D} \tag{9}$$

where $(m/A)_a$ is the average m/A over the fragment m/A distribution.

Combining Eqs. 2 and 3 with the approximation $S_B = S_f$ gives the equilibrium spatial density of fragments as

$$S_B = \frac{S_i^2 \sigma_i V\,\Delta U \int S_1(t)\,dt}{1 - S_i \sigma_i V\,\Delta U \int S_1(t)\,dt} \tag{10}$$

As $S_i \sigma_i V\,\Delta U \int S_1(t)\,dt$ approaches 1, S_B tends to infinity. Also $S_i \Delta U = N_i$, the number of intact objects above h_1. Therefore, after combining with Eq. 9, the critical number of intact objects above h_1 producing a runaway environment is

$${}_R N_i = \frac{4\pi a^3 V_o \rho_a C_D}{N_0 W (m/A)_a V \sigma_f} \tag{11}$$

where, if r_e is the radius of the earth, $a = r_e + h_1$.

The threshold for an unstable environment depends upon the current fragment population. The question is whether the current fragment population will increase due to random collisions alone. The answer is found by setting the current fragment population equal to S_B in Eq. 10 and solving for the value of S_i that produces an equilibrium equal to the current fragment population. In [1], the current fragment population was defined as a factor, k, applied to the intact population. That is, $S_f = S_i/k = S_B$. Hence, the critical number of intact objects above h_1 producing an unstable environment is

$${}_U N_i = \frac{{}_R N_i \sigma_f}{\sigma_f + k\sigma_i} \tag{12}$$

4 RESULTS

Reference [1] adopted the following values for the LEO regions below 1020 km: $N_0 = 90$, $(m/A)_a = 125$ kg/m^2, $\sigma_f = 14$ m^2, $\sigma_i = 53$ m^2, $W = 1.1$, $C_D = 2.2$, and $k = 2$. Atmospheric densities used in [1] were from NASA SP-8021 under the assumption of an average solar activity of 130, representing an exospheric temperature of 980 K after accounting for geomagnetic activity. The number of intact objects found between the given altitude and an altitude of 1020 km was estimated by multiplying the spatial density by volume to obtain the number, then summing between 1020 km and the given lower altitude, producing the plot in Fig. 1 above.

Here, atmospheric densities were found from the CIRA-72 atmospheric model under the same assumption of average solar activity. Additionally, the effective number of intact objects found between the given altitude and an altitude of 1020 km was calculated from data retrieved from the Space-Track catalogue. The summation between 1020 km and the given lower altitude was conducted for altitude bins of 10 km size. With these differences, Fig. 14 shows the number of intact objects in the catalogue during February 1999 and the corresponding threshold numbers for a runaway environment and for an unstable environment, using the model values listed above from [1]. To aid comparison, a smaller version of Fig. 1 is shown as inset within Fig. 14. Differences in the two plots are accounted for by the use of different atmospheric models, intact object population data and the binning approach. The region between 800 km and 1000 km is above the runaway threshold and region between 600 km and 1000 km is well above the unstable threshold.

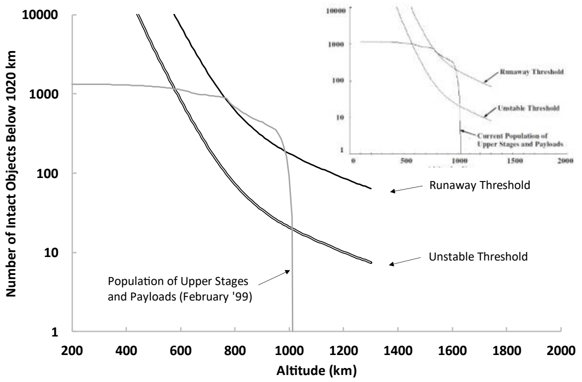

Figure 14. Regions of Instability Below 1020 km for the February 1999 Population Using Stability Model Parameters from [1]. Inset Figure Shows the Result from [1].

Analysis of the additional collision data presented above and use of the average cross-sectional area data for intact objects in orbit on 1 February 1999 from ESA DISCOS suggest the use of the following model values for the LEO regions below 1020 km: $N_0 = 112$, $(m/A)_a = 102$ kg/m^2, $\sigma_f = 12$ m^2, and $\sigma_i = 36$ m^2, with other values remaining unchanged. A comparison of the resulting threshold numbers for runaway and unstable environments with those obtained using the original model values is shown in Fig. 15. The combination of some factors that raise the threshold (σ_f, σ_i) and factors that lower the threshold (N_0, $(m/A)_a$) ultimately lead to relatively little change to the thresholds overall compared with the results in [1].

Average cross-sectional area data from the DISCOS database for intact objects in orbit on 1 February 2025 indicate the following model values for use with the current population: $\sigma_f = 18$ m^2 and $\sigma_i = 60$ m^2. Fig. 16 is a plot of the number of intact objects from the 28 March 2025 population found between the given altitude and an altitude of 1020 km. This figure shows there are over 12,000 intact objects below 1020 km, many of which are associated with a single operator, with about 10,000 objects between 450 km and 1020 km. All altitudes between 420 km and 1000 km are substantially above the unstable threshold. The region between 520 km and 620 km is now at or above the runaway threshold, while all regions between 620 km and 1000 km are substantially above it. Where this is the case, maintaining the population of intact objects will cause the fragment population to increase to an infinite number over an infinite amount of time.

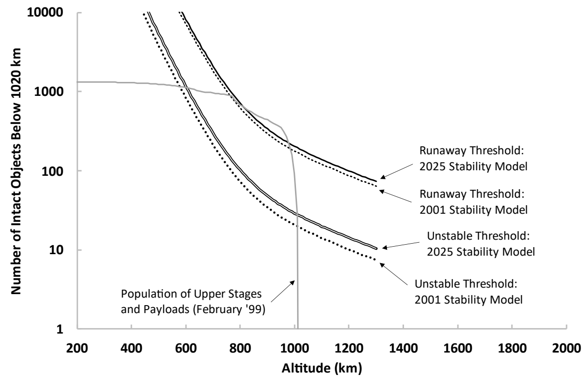

Figure 15. Comparison of the Runaway and Unstable Thresholds for the Original Stability Model Parameters from [1] and the Updated Model Parameters.

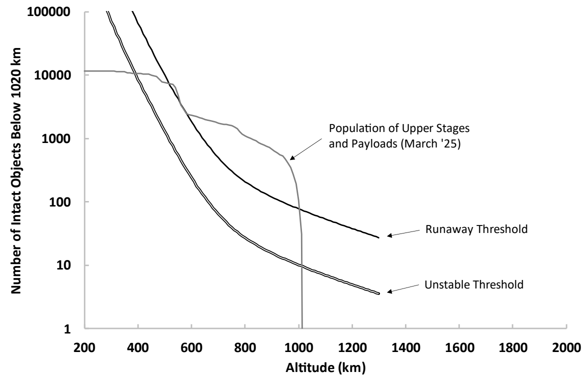

Figure 16. Regions of Instability Below 1020 km for the March 2025 Population of Intact Objects Using Updated Stability Model.

4.1 Implications of upper stage breakup data

Reference [1] found that payloads were nearly 10 times more important than upper stages in causing instabilities in the environment. They concluded that upper stages could nearly be ignored and that, by doing so, the model values could be adjusted to reflect a "best case" because the upper stages were larger than the payloads – i.e., the average collision cross-sections would be reduced if the upper stages were ignored. Under this assumption, [1] found that none of the environment below 1020 km was above the runaway threshold.

However, cross-sectional area data from ESA's DISCOS database indicate that below 1020 km the average payload is now larger than the average upper stage. Consequently, ignoring the upper stages would lead to the following model values: $\sigma_f = 19$ m^2 and $\sigma_i = 61$ m^2. Fig. 17 then represents the "best case" arising by ignoring the upper stages. In contrast to [1], the regions of instability remain more-or-less unchanged. The region between 620 km and 1000 km is still substantially above the runaway threshold and the region between 520 km and 600 km remains close to or above it. All altitudes between 420 km and 100 km remain above the unstable threshold.

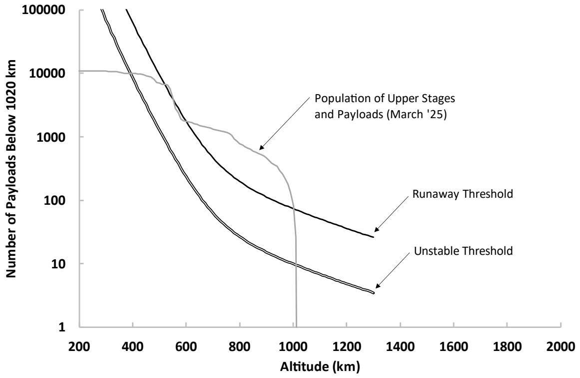

Figure 17. "Best Case" Regions of Instability Below 1020 km for the March 2025 Population of Intact Objects Using Updated Stability Model.

Even in this "best case", the expectation for the near future is for an accelerating launch rate and a corresponding increase in the number of intact objects below 1020 km, rather than a reduction in this number. This growth will be dominated by constellations deployed to this part of LEO.

4.2 Implications of planned constellations

Based on a review of International Telecommunications Union (ITU) filings, [12] suggested that "a dramatic increase in satellite numbers is possible, much more than the tens of thousands often reported." Using the ITU's "as received database" for the period 1 January 2017 to 31 December 2022, the authors found filings for more than 300 constellations, each with 10 or more satellites and 90 with more than 1000 satellites, representing more than 1 million satellites in total. Many of these satellites will be deployed to altitudes in LEO below 1020 km, the region of interest here.

Fig. 18 plots the population of intact objects for March 2025, the regions of instability calculated using the stability model (note these are not the "best case" regions), and the destination altitudes for some of the large constellations that are planned or are currently being deployed. The figure shows that many satellites are expected to enter the region currently at or close to the runaway threshold between 520 km and 620 km, while several constellations are planned for the region between 620 km and 1000 km that is already above the runaway threshold. Additionally, the large numbers of satellites expected to be deployed at altitudes below 420 km, some in Very Low Earth Orbit (VLEO), may increase the population over the unstable threshold.

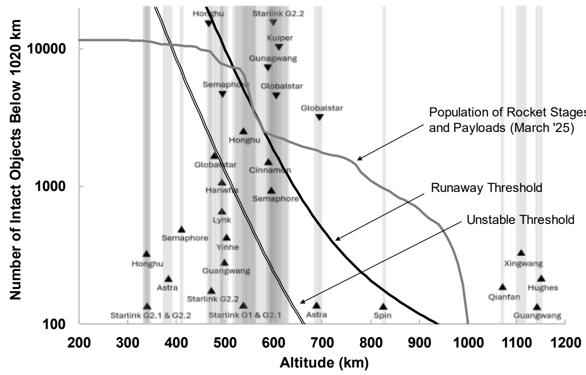

Figure 18. Destination Altitudes for Some Planned Large Constellations of Satellites and Regions of Instability for the March 2025 Population of Intact Objects. Constellation Data from Jonathan McDowell's Space Pages with Some Minor Amendments.

One of the many factors determining the orbital altitude for constellations, particularly those providing communications services, is latency. Operating at low LEO altitudes and at VLEO altitudes reduces the latency, offering communication speeds that rival ground-based fibre. This benefit is traded off against the increasing number of satellites needed to achieve the coverage requirements and the impacts of a much higher atmospheric density. Whilst the high density will tend to mean that finite propellant resources onboard low LEO and VLEO satellites are consumed more rapidly than satellites at higher altitudes, there are also potential benefits with respect to space debris mitigation and space sustainability. At such low altitudes, the residual orbital lifetimes will be measured in months or just a few years – well below the residual orbital lifetimes required by the US Federal Communications Commission (FCC) and other regulators. Additionally, fragments from any collisions occurring will also have very short residual lifetimes, leading to a perception that such low-altitude operations are more sustainable than those at higher altitudes [13].

The results presented above suggest these perceived benefits for constellations at low LEO altitudes may not be realised. The large numbers of satellites within these constellations and the extended period over which the constellations are maintained by replenishing satellites – potentially over many decades – will mean that an unstable or even runaway environment at low LEO altitudes will continue to be a possibility.

Some moderation of this risk may be achieved through use of collision risk mitigation manoeuvres (so-called "collision avoidance manoeuvres"), if there is the capability to perform orbital changes in a timely fashion, if conjunction alerts arrive with sufficient warning time, and if these alerts are derived from accurate and reliable sensor or operator data. However, ground-commanded or semi- or fully-autonomous collision avoidance manoeuvres are limited by:

1. Size limitations for all tracking radars, whether SSN-related or via commercial vendors. Satellite breakups can occur for projectiles below the physical limitations (detection, correlation between observations) or practical limitations (e.g. sufficient knowledge to promote into the public catalogue).
2. Delays for the first orbital elements of the fragments of a breakup to enter the public catalogue, even for large events in relatively sparse regions of space.
3. Manoeuvring satellites reducing the accuracy of situational awareness, thereby reducing the reliability of future conjunction warnings [14].
4. Residual, "ignored", or "accepted" collision probability remaining high for large constellations of satellites even if many manoeuvres are made at relatively low-collision-probability thresholds [15].

Some data suggest that the real-world effectiveness of collision avoidance manoeuvres does not match many expectations [16]. Hence, whilst it may be argued that collision avoidance manoeuvre capability should be included in the model values used to identify the "best case" regions of instability below 1020 km, the uncertainty over the actual benefit mean that such modification is as-yet unjustified.

5 CONCLUSIONS

The intentional collision breakup of the Fengyun-1C satellite, the accidental collision of Iridium-33 with Cosmos-2251, and a new ground-based hypervelocity impact test have enabled an update to the work previously reported by Kessler and Anz-Meador in [1]. In combination with data from the P-78 orbital satellite test and the Transit ground-based test, an analysis of these collisions has confirmed the previous findings that large regions of low Earth orbit were unstable, leading then to an expectation of an increasing fragment population due to random collisions. In the "best case" evaluated by Kessler and Anz-Meador, which excluded upper stages in the February 1999 population, the increase would likely have levelled off and reached a new, higher equilibrium level. However, inclusion of the upper stages may have prevented an equilibrium environment being reached in the region between 800 km and 970 km.

The current (March 2025) population of intact objects is now above the threshold for an unstable environment at altitudes between 420 km and 1000 km, based on updated stability model values from the additional orbital collisions and a new ground-based test. As before, this instability will cause a slowly increasing fragment population across a broad range of LEO altitudes. Furthermore, the threshold for a runaway environment has now been exceeded or is close to being exceeded at altitudes between about 520 km and 1000 km, even if upper stages are ignored.

The continuing absence of hypervelocity breakup data for upper stages and the underestimation of fragment sizes in the decimetre range from SSN-derived RCS measurements are limitations in the current work. However, the differences between the 2001 and 2025 "critical numbers" are relatively small – it is the significant change in the population of intact objects below 1000 km over the last two decades that has driven the expansion of the regions of instability.

The current intact population is increasing at an unprecedented rate, with ITU filings suggesting more than 1 million satellites could enter orbit in the near future. Many of these new satellites will form large constellations of satellites, with several targeting the regions of instability identified. Despite the mitigation potential arising from collision avoidance manoeuvres, the rate of increase in collision fragments will increase substantially. As noted already in [1], and reinforced by the results presented above, these conditions mean that after some period of time – perhaps shorter than previously anticipated – the intact population would be difficult to maintain because the fragment population would become too hazardous to continue space operations in low Earth orbit. This finding has implications for large constellations already in orbit and those that are planned.

Whilst these conclusions are not too different from those of previous studies and point to instabilities that are likely anticipated in the context of a possible 1 million satellites, they serve to emphasise the importance and timeliness of limiting future breakups in space and of identifying management tools that address the environmental conditions leading to instability.

6 ACKNOWLEDGEMENTS

The research presented in this paper made use of information from Space-Track.org, KeepTrack.space, maintained by Theodore Kruczek (Founder), Jonathan McDowell's Space Pages, and ESA DISCOS (Database and Information System Characterising Objects in Space). We acknowledge the use of these databases, and the efforts of the teams and individuals involved in their maintenance and operation. The authors would also like to thank Sam Diserens for an important contribution with respect to the data gathering and processing, and a colleague at NASA for their guidance and support throughout the research.

7 REFERENCES

1. Kessler, D.J. & Anz-Meador, P.D. (2001). Critical Number of Spacecraft in Low Earth Orbit: Using

Satellite Fragmentation Data to Evaluate the Stability of the Orbital Debris Environment. In Proc. 3rd European Conference on Space Debris, ESA SP-473, pp265-272.

2. Liou, J.-C. & Johnson, N.L. (2006). Risks in Space from Orbiting Objects. *Science*, **311**(5759), 340-341.

3. Lewis, H.G. (2020). Understanding Long-Term Orbital Debris Population Dynamics. *J. Space Safety Eng*., **7**(3), 164-170.

4. Weeden, B. (2010). 2007 Chinese Anti-Satellite Test Fact Sheet. Secure World Foundation. Online at https://swfound.org/media/9550/chinese_asat_fact_sheet_updated_2012.pdf (as of 22 March 2025).

5. Weeden, B., (2010). 2009 Iridium-Cosmos Collision Fact Sheet. Secure World Foundation. Online at https://swfound.org/media/6575/swf_iridium_cosmos_collision_fact_sheet_updated_2012.pdf (as of 22 March 2025).

6. Murray, J., Blackwell, C., Gaynor, J. & Kennedy, T. (2019). Haystack Ultra-Wideband Satellite Imaging Radar Measurements of the Orbital Debris Environment: 2014-2017. NASA Technical Report TP-2019-220302, NASA Johnson Space Center, Houston, TX, USA.

7. Johnson, N.L., Krisko, P.H., Liou, J.-C., & Anz-Meador, P.D. (2001). NASA's New Breakup Model of EVOLVE 4.0. *Adv. Space Res*., **28**(9), 1377-1384.

8. Anon. (2022). The Intentional Destruction of Cosmos 1408. *Orbital Debris Quarterly News*, **26**(1), 1-5. Online at: https://www.orbitaldebris.jsc.nasa.gov/quarterly-news/pdfs/ODQNv26i1.pdf (as of 22 March 2025).

9. Murray, J., Cowardin, H., Liou, J.-C, Sorge, M., Fitz-Coy, N. & Huynh, T. (2019). Analysis of the DebriSat Fragments and Comparison to the NASA Standard Satellite Breakup Model. In Proc. 1st International Orbital Debris Conference, Technical Report No. JSC-E-DAA-TN73918, NASA Johnson Space Center, Houston, TX, USA.

10. McKnight, D.S., Maher, R. & Nagl, L. (1992). Fragmentation Algorithms for Satellite Targets (FAST) Empirical Breakup Model Version 2.0. DOD/DNA Orbital Debris Spacecraft Breakup Modeling Technology Transfer Program, Kaman Sciences Corporation.

11. Kessler, D.J. (1990). Collision Probability at Low Altitudes Resulting from Elliptical Orbits. *Adv. Space Res*., **10**(3-4), 393-396.

12. Falle, A., Wright, E, Boley, A. & Byers, M. (2023). One Million (Paper) Satellites. *Science*, 382(6667), 150-152.

13. Lewis, H.G. (2020). Evaluation of Debris Mitigation Options for a Large Constellation. *J. Space Safety Eng*., **7**(3), 192-197.

14. Oltrogge, D.L., Cornelius, J.J., Glinski, T.J., Vallado, D.A., Alfano, S., Hall, R.A., Chan, J.C., Law, C. & Ridgeway, A. (2023). Addressing the Debilitating Effects of Maneuvers on SSA Accuracy and Timeliness. In Proc. Advanced Maui Optical and Space Surveillance Technologies Conference (AMOS), Maui, Hawaii, USA.

15. Lewis, H.G. & Skelton, G. (2024). Safety Considerations for Large Constellations of Satellites. *J. Space Safety Eng*., **11**(3), 439-445.

16. Shepperd, R. (2024). How to Categorize an Avoidance Maneuver: Untangling the Iridium Experience. In Proc. Advanced Maui Optical and Space Surveillance Technologies Conference (AMOS), Maui, Hawaii, USA.